Ground, airborne, and satellite measurements of fire radiative power—RxCADRE 2012

Matthew B. Dickinson[A,K], Andrew T. Hudak[B], Thomas Zajkowski[C,L], Louise E. Loudermilk[D], Wilfrid Schroeder[E], Luke Ellison[F,G], Robert L. Kremens[H], William Holley[I], Otto Martinez[I], Alexander Paxton[I], Benjamin C. Bright[B], Joseph J. O'Brien[D], Benjamin Hornsby[D], Charles Ichoku[F], Jason Faulring[H], Aaron Gerace[H], David Peterson[J], and Joseph Mauceri[H]

[A]USDA Forest Service, Northern Research Station, 359 Main Road, Delaware, OH 43015, USA

[B]USDA Forest Service Rocky Mountain Research Station, Forestry Sciences Laboratory, 1221 South Main Street, Moscow, ID 83843, USA

[C]USDA Forest Service, Remote Sensing Applications Center, 2222 W. 2300 South Salt Lake City, UT, 84119 USA

[D]USDA Forest Service, Center for Forest Disturbance Science, Southern Research Center, 320 Green St., Athens, GA 30602, USA

[E]Department of Geographical Sciences, University of Maryland, College Park, MD 20742, USA

[F]NASA Goddard Space Flight Center, Greenbelt, MD 20771, USA

[G]Science Systems and Applications, Inc., Lanham, MD 20706, USA

[H]Rochester Institute of Technology, Center for Imaging Science, 54 Lomb Memorial Drive, Rochester, NY 14623

[I]US Air Force, 96th Test Wing, Eglin Air Force Base, Niceville, FL 32542, USA

[J]National Research Council, 7 Grace Hopper Ave, Monterey, CA 93943, USA

[K]Corresponding author. Email: mdickinson@fs.fed.us

[L]Current address: Institute for Transportation Research and Education, North Carolina State University, Raleigh, NC 27695, USA

Abstract

Characterizing radiation from wildland fires is a focus of fire science because radiation relates directly to the combustion process and can be measured across a wide range of spatial extents and resolutions. We compared ground, airborne, and satellite retrievals of fire radiative power (FRP) over entire fires as a means of validating measurements and developing an understanding of their limitations. Coincident measurements of fire power were made on small (2 ha) and large (more than 100 ha) burn blocks during the Prescribed Fire Combustion and Atmospheric Dynamics Research (RxCADRE) project in 2012. On small fires, FRP estimated from an obliquely-oriented longwave infrared camera mounted on a boom lift were compared with FRP derived from combined data from tower-mounted radiometers and remotely-piloted aircraft systems. Results suggest a bias in measurements the source of which is unclear. For large fires, satellite FRP estimates, generated from the MODIS and VIIRS sensors, were compared with FRP derived from a longwave infrared imaging system aboard a piloted aircraft. Discrepancies highlight the need for continued development and evaluation of fire remote-sensing measurements.

Summary

Remotely-sensed wildland fire radiation is an important measurement target for fire science but comparisons among measurement methods are needed. We compare ground, airborne, and satellite measurement of radiative power over whole fires. Comparisons highlight measurement

bias and uncertainty and suggest that we as yet have no "gold standard" fire radiated power measurement.

Introduction

The primary purpose of this paper is to describe methods by which to derive measurements of fire radiative power (FRP) across entire burns using ground-, airborne-, and satellite-based sensors, and to compare those measurements and explore their strengths and limitations. Satellites that quantify infrared emissions from wildland fires hold great promise as methods for long-term monitoring of active fires, fuel consumption, and smoke production (e.g. Coen and Schroeder 2013; Schroeder *et al.* 2013, 2014; Peterson *et al.* 2013; Peterson and Wang 2013; Freeborn *et al.* 2014). Satellite measurements, however, are subject to limitations and these can be explored and quantified through ground (e.g. Kremens *et al.* 2012) and airborne (e.g. Riggan *et al.* 2004; Peterson *et al.* 2013, 2014) measurements at higher spatial and temporal resolution. Ground and airborne measurements, however, also have their challenges, including limitations on replication and spatial extent and the lack of fundamental knowledge of fire radiation (Kremens *et al.* 2010).

There is no "gold standard" wildland FRP measurement, only measurements of fire radiation for which we more or less understand accuracy, precision, and uncertainty. Only recently has a comparison among ground, airborne, and satellite data from an active fire been achieved (Schroeder *et al.* 2013) in which ground radiometer measurements of FRP were similar to airborne measurements and, in turn, airborne measurements coincided with measurements from four spaceborne sensors, including the GOES geosynchronous imagers (East and West). The GOES imagers provided data at a temporal resolution similar to that of an airborne sensor making repeated passes over a fire, albeit at a much coarser spatial resolution (>6 km). Understanding the accuracy and precision of fire radiation measurements and improving those measurements is paramount to the future use of airborne and satellite measurements for fire behavior characterization and ecological effects prediction (Kremens *et al.* 2010).

In this paper, we focus on whole-fire FRP measurement because that scale best corresponds to the spatial resolution of current satellites designed for fire detection and quantification. We describe four independent methods of measuring FRP over entire prescribed fires. On small burn blocks (2 ha), we compare oblique, boom-mounted longwave infrared (LWIR) camera measurements of FRP with those derived from data from tower-mounted radiometers and remotely-piloted aircraft systems (RPAS). On large burn blocks (>100 ha), we report measurements from the Wildfire Airborne Sensor Program (WASP) platform flown on a fixed-wing, piloted aircraft, and compare those measurements with FRP estimated from two spaceborne sensors, the Suomi-National Polar-orbiting Partnerships' Visible Infrared Imaging Radiometer Suite (VIIRS), and the Earth Observing System Moderate-resolution Imaging Spectroradiometer (MODIS) instrument. Data are from the 2012 RxCADRE experiments on Eglin Air Force Base in northwestern Florida (see Ottmar *et al.*, this issue).

Background and methods

Burns reported in this paper were conducted at Eglin Air Force Base on Range B70 in late 2012 and included small and large blocks dominated by herbaceous and shrub fuels and one large forested block (details in Ottmar *et al.*, this issue). Burn blocks are shown in Fig. 1. Following, four independent methods of estimating whole-fire FRP are described.

Fire radiative power from RPAS and nadir-viewing radiometers

RPAS are receiving increasing interest in fire operations and science applications but experience in their use is limited. The RxCADRE project offered the opportunity to assess capabilities and data products (Zajkowski *et al.*, this issue). Here, we report the methods by which whole-fire FRP for small burn blocks was derived using a combination of RPAS and radiometer data. FRP was calculated as the product of perimeter length (m) estimated from RPAS imagery and frontal radiant intensity (kW m^{-1}) estimated from radiometers. Nadir-viewing, dual-band radiometers (termed radiometers hereafter) were distributed at 10-m intervals from a central meteorological tower. Surveyed locations of these instruments are provided in the RxCADRE data archive (US Department of Agriculture, Forest Service Research xxxx). Radiometers were attached to a 0.5-m arm and elevated to 5.5 m on telescoping poles anchored to steel fenceposts (see Kremens *et al.* 2010, 2012, and 2014 for details on data analysis, calibration, and use). Voltages were logged at 5-s intervals from which average fire radiative flux density (FRFD) (W m^{-2}) was calculated. The sensors used in the radiometers were built by Dexter Research. The longwave sensor (detector ST60 DX-0852) has a silica window with a nominal bandpass of 6.5 to 20 µm (spectral transmission described by DC-6186-L2). The midwave sensor (detector ST60 DX-0852) has a calcium fluoride window with nominal bandpass of 3 to 5 µm (spectral transmission described by DC-6100-CaF_2-U8). The field of view of the sensors was 24° at 50% response (i.e. full width at ½ maximum response) (FWHM). FRP was calculated from peak FRFD through multiplication by the sensor's FWHM field of view on the ground (m^2). Flame fronts were assumed to be linear within the field of view, and FRP was divided by the diameter of the field of view to estimate average fire radiant intensity in Wm^{-1} in analogy to frontal fire intensity (Byram 1959).

Flame-front perimeters were estimated from RPAS LWIR data. Frames encompassing entire blocks were captured by a FLIR Tau 640 camera (nominal 8- to 14-µm bandpass) mounted obliquely on a small RPAS (the G2R) that orbited the block. The frames were orthorectified with reference to infrared "hot" targets and features visible on high resolution aerial orthophotos. Specifications of the FLIR Tau camera and G2R are provided in Zajkowski *et al.* (this issue). The RPAS frames were used to identify flame fronts whose perimeters were manually delineated after image classification. It was found that RPAS images from a similar perspective (collected as the G2R aircraft orbited the fire) were required to obtain consistent perimeters from orthorectified frames as fires spread. Perimeters were somewhat ambiguous when flame fronts were not continuous, that is, when the flame front extinguished in certain areas. In these cases, discontinuous perimeters were added to estimate total perimeter.

Fire radiative power estimated from oblique LWIR data

High-resolution LWIR cameras have been used to provide a nadir perspective of flaming combustion for ecological effects research, but their use to quantify fire dynamics is limited (see O'Brien *et al.*, this issue). A LWIR camera elevated on a boom lift (FLIR SC660) with a nominal bandpass of 7.5 to 13 µm was used to measure fire progression and FRFD from an oblique perspective. Thermal images were captured at 1Hz, emissivity was set at 0.98, and temperature range was set to 300 to 1500°C. Further information on FLIR specifications and image rectification and processing are found in Hiers *et al.* (2009), Loudermilk *et al.* (2012), and O'Brien *et al.* (this issue). Orthorectified image data were rendered at 1-m^2 scale and these data were integrated spatially to provide whole-fire radiated power (FRP) (MW). A 25-m boom lift, fully extended and located 10 to 25 m outside of each block's boundary, was used to elevate the camera.

Fire radiative power estimated from airborne LWIR data

Airborne infrared imaging can provide relatively high-resolution data over spatial scales typical of entire prescribed fires, thus providing data that can be used to evaluate and understand satellite data (e.g. Schroeder *et al.* 2013). Longwave imagery was captured by the Wildfire Airborne Sensor Program (WASP) sensor during repeated passes over each of the three large burns. Midwave infrared imagery are also available from the WASP system, but saturation and reflected solar radiation limit their use. The WASP system is described in McKeown *et al.* (2004), and its utility is described in Ononye *et al.* (2007). The WASP Indigo Phoenix LWIR camera (model IA126 LWIR) was built by Cantronic Systems Incorporated and has quantum-well, cooled detectors. Peak transmission is at 8.7 µm with a nominal bandpass of 8 to 9.2 µm. Flight altitude was determined in part by compromise between the goals of capturing entire blocks in a single mosaic of frames captured on a single pass and the need to fly below any existing cloud deck. The general calibration method, combining laboratory calibration, fire radiation simulations, and the spectral response of the system, is described in Kremens and Dickinson (2014, Accessory Publication 1). Because atmospheric absorption varies with flight altitude and atmospheric conditions, we used the Moderate Resolution Atmospheric Transmission code (MODTRAN) (Berk *et al.* 2003) to estimate spectral absorption, which was incorporated in the calibration process. An automated process based on Applanix inertial measurement unit data was used to orthorectify image frames. Canopy interception of radiation is a known limitation of both airborne and satellite measurements of fire radiation, but no correction was attempted for our forested block (Hudak *et al.*, this issue). Cloud cover ranged from 0 to 10% for L1G, averaging ≤5%. Although affecting satellite measurements (see *FRP estimated from spaceborne sensors*, below), the cloud deck was higher than the WASP flight altitude for L2F.

FRP estimated from spaceborne sensors

Among the set of active fire imaging sensors (e.g. Schroeder *et al.* 2013), only the daytime (from midday to early afternoon) overpasses from MODIS on the EOS/Aqua satellite, a standard in FRP retrieval in the fire science community, and the VIIRS sensor, borne on the S-NPP polar satellite (launched in 2011) provided sufficient opportunity to observe the experimental fires given RxCADRE research priorities and operational constraints. Both satellites follow a similar orbit (Justice *et al.* 2013; Csiszar *et al.* 2014) and their timing is convenient for coordination with prescribed fire operations.

MODIS

MODIS fire detection (e.g. Justice *et al.* 2002) is accomplished using the spectral bands centered at ~4 μm (midwave) and ~11 μm (longwave), although data from several other spectral bands are also utilized for masking clouds, extremely bright surfaces, glint, and other potential sources of false detection (Giglio *et al.* 2003). The official MODIS fire data product provides data sets of detected fire pixels at 1 km resolution and their respective FRP values calculated only from the ~4 μm measurements (Kaufman *et al.* 1998; Justice *et al.* 2002, 2006; Giglio *et al.* 2003). MODIS overpasses were coincident with experiments S6, L1G, L2G and L2F on 31 October and 4, 10, and 11 November 2012, respectively (Table 1). The MODIS active fire product (MYD14) retrievals for these overpass events were collected, and the radiance data were corrected for atmospheric absorption using MODTRAN 4v3 (Berk *et al.* 2003) and atmospheric profiles derived from National Centers for Environmental Prediction 0.5° resolution 6-hourly data. An average atmospheric absorption weighted by sensor spectral response was used to correct top of the atmosphere values to give ground-leaving FRP (Table 1).

Only L2G and L2F recorded fire detections based on MYD14 with two pixels registered for the L2G plot, and four pixels for the L2F plot. However, because of MODIS scanning design and the fact that ground pixel size increases away from nadir, it is possible to have duplicate detections of the same fire as a result of *bow-tie* distortion affecting pixels acquired at scan angles greater than ~25 ^{o} (Wolfe et al, 2002). This was the case for L2F where two neighboring scans both detected the same fire on the ground. In this case, simply summing the FRP values from both scans would result in an overestimation of overall FRP. Instead, because the first scan only partially detected the fire with one registered fire pixel, the three FRP values from the subsequent scan, which did cover the entire L2F plot, were used to estimate total FRP.

Fires S6 and L1G were coincident with MODIS image acquisition but not detected (Table 1). MODIS's view angle for burn S6 was large (51.2°), whereas the active fire area was small (much less than the 2 ha burn block's area) relative to the pixel's 6.2 km^2 footprint (Table 1). Consequently, the fire's radiative signal was too weak to be separated from the background. Meanwhile, inspection of the MODIS metadata coinciding with L1G showed that the corresponding fire signal was discarded due to the detection of opaque clouds over the experimental fire. FRP for L1G was calculated manually and included in Table 1 with the proviso that the resulting FRP value for L1G will likely underestimate true FRP.

Because the prescribed-fire unit boundaries were known, we were able to provide lower and upper bounds on FRP. The lower bound is the summation of individual-pixel values whose FRP rose above background. The upper bound is the summation of FRP from all pixels that overlapped unit boundaries. A detailed discussion of methods is provided in Ellison and Ichoku (2014, Accessory Publication 2).

VIIRS

VIIRS is a multispectral instrument supporting Earth weather and climate applications and launched in 2012. Full global coverage is accomplished every 12 h or less using two distinct sets of spectral channels at 375-m (Schroeder *et al.* 2014) and 750-m nominal resolution. A unique data aggregation scheme was applied to the sensor's radiometric data in order to limit pixel area increase along scan, thereby resulting in greater image integrity compared to other wide-area orbital scanning systems (Wolfe *et al.* 2013). The 750-m data set includes a dual-gain midwave infrared (MIR) channel with a high saturation temperature of 634 K designed to detect and characterize active fires (Csiszar *et al.* 2014).

VIIRS coincidently imaged S5, L1G, L2G, and L2F during firing operations (Table 2). Automated active fire detection data were produced for the 375-m and 750-m data sets using the methodologies described in Schroeder *et al.* (2014) and Csiszar *et al.* (2014), respectively. The 375-m active fire product detected all four fires, whereas the 750-m product detected only L2G. The cause for omission errors in the 750-m product were mainly due to the small size of the S5 fire resulting in weak radiative signal in the primary MIR detection channel, and the presence of scattered opaque clouds over L1G and L2F causing partial fire obscuration with consequent classification of the area as cloud-covered. Because of the low saturation temperature (367 K) of the 375-m MIR channel driving that active fire algorithm, the larger fires at L1G, L2G, and L2F resulted in saturated pixel radiances (Table 2). Meanwhile no pixel saturation was found in the higher saturation temperature (634°K) 750-m data.

To overcome the limitations imposed by fire omission errors and pixel saturation described above, VIIRS 375- and 750-m coincident data were used interchangeably (Table 2). Fire-affected pixels omitted by the 750-m product were accounted for using co-located reference pixels detected by the 375-m product. Pixel-based FRP retrievals were derived using the method by Wooster *et al.* (2003) applied to unsaturated MIR (single-band) radiance data only. Hence, two separate FRP retrievals were produced using the 375- and 750-m data for block S5, whereas single retrievals based on 750-m radiance data were produced for blocks L1G, L2G, and L2F. VIIRS MIR radiance data were corrected for atmospheric attenuation using the MODTRAN code as described above.

Results and discussion

FRP from RPAS and nadir-viewing radiometers

An example set of RPAS-derived perimeters is shown in Fig. 2. Estimates of FRP estimated from RPAS and radiometers are shown in Table 4. Fire perimeters ranged from 114 to 1197 m and frontal radiant intensity ranged from 10.9 to 54.7 kW m^{-1}. Whole-burn FRP, the product of fire perimeter and frontal radiant intensity, ranged from 2.2 to 30.7 MW.

FRP estimated from oblique LWIR data

The oblique (rectified) LWIR imagery showed temporal and spatial fluctuations in FRP that appeared to be caused by variation in fuels and changing wind speed and direction (See O'Brien *et al.*, this issue). Mean FRP averaged across each fire ranged from 1.2 to 5.1 MW and area burned ranged from 0.5 to 2.3 hectares (Table 3). An example time-course of oblique, whole-fire FRP is shown Fig. 3.

FRP estimates from airborne LWIR data

Fire radiated power over time for large fires generated from airborne LWIR data is shown in Fig. 4. Peak FRP was highest for the forested burn and the duration of the ignition operations and heat release from the fire were also longer than for the non-forested blocks. Estimates of background FRFD from radiometers were used to establish a background threshold for FRP calculation. This background, averaging 1070 W m^{-2} (with a 95% confidence interval of 863–1288 W m^{-2}) was the asymptote to which FRFD approached after flame fronts spread below instruments. More information on airborne infrared FRP calculations and their integration to estimate fire radiative energy are given in Hudak *et al.* (this issue).

FRP estimates from spaceborne sensors

Ground-leaving FRP estimates from MODIS (corrected for atmospheric absorption) for three large fires ranged from 110 to 215 MW (Table 1). MODIS FRP is also shown in Figs. 4 and 6 along with FRP calculated from airborne LWIR data. A range of estimates were obtained for each fire based on different ways of treating the background and whether flagged fire pixels or clusters of pixels that overlapped the burn blocks were used as the basis for FRP determination (see Ellison and Ichoku 2014, Accessory Publication 2, for details). The MODIS pixel grid for L2F is shown in Fig. 5 over a near-coincident WASP mosaic. Images showing cloud cover at the time of L1G retrieval are shown in Ellison and Ichoku (2014, Accessory Publication 2).

Ground-leaving FRP estimates from VIIRS data for the three large fires ranged from 151 to 237 MW (Table 2). VIIRS pixels included in the FRP estimate for L2F overlay a near-coincident WASP mosaic in Fig. 5. Scan angles ranged from 3 to 30 degrees. All three large fires were detected from the 375-m nadir resolution data (realized pixel area of 0.1 to 0.3 km^2). The fire at site L2G was the only one detected by the coarser 750-m data at near-nadir observation conditions (3.2° scan angle) and 0.56 km^2 effective pixel area. Representative VIIRS pixels overlaying WASP FRP imagery are shown in Fig. 5. Small fire S5 coincided with a VIIRS overpass and was detected by the 375-m data at a 41.5° scan angle at 350-m nadir resolution with no saturation.

Comparisons among FRP measurements reveal limitations

Coincidence among airborne WASP and satellite measurements is shown in Figs. 4 and 6 and Table 5. Comparisons are qualitative because of low replication. Airborne infrared estimates of whole-fire FRP were higher than those for VIIRS (average difference of 169 MW) except for L2G for which the VIIRS estimate was within 1 MW of WASP (Table 5 and Fig. 6). For the L1G and L2F fires, cloud cover was present and may have attenuated the radiation reaching the VIIRS sensor. For L1G, at the time of VIIRS overpass, cloud cover estimated from WASP imagery was ~2% (Table 5). The midpoint of pixel and cluster estimates of FRP from MODIS were within 43 MW of WASP estimates on average (Table 5 and Fig. 6). Cloud cover likely reduced the MODIS estimate of FRP for L1G and was about 5% at the time of MODIS overpass as estimated from near-coincident WASP imagery. For cloud-affected FRP estimates, WASP estimates were not consistently higher.

RPAS-based estimates of FRP were significantly related to FRP estimated from oblique LWIR by linear regression, but RPAS estimates were higher (Fig. 7). The regression relationship in Fig. 7 is strongly influenced by the largest RPAS-based estimates of FRP (for S3 and S7), illustrating that more replication for high-FRP fires would have been desirable. The imagery from the RPAS-borne FLIR Tau 640 exhibited “blooming” (see below) which may have resulted in inflated perimeter estimates and, thus, FRP. From other data (see Butler *et al.*, this issue), we know that radiometers in block S5 described a mix of heading fire and lower intensity, less organized flame fronts. As such, the mix of fire behavior sampled by radiometers for S5 does not appear to be biased towards heading behavior and, thus, high fire radiant intensity. Replication of radiometer measurements (N ranged from 4 to 5) was low for small blocks which must increase error and uncertainty for RPAS-based estimates of FRP.

A clear limitation of using small RPAS for fire research is the low quality of both the infrared sensors and the navigation data required to rectify the imagery. Because infrared cameras available currently for small RPAS are designed to detect low-temperature objects, they saturate at the high radiant flux densities associated with fires. Another limitation is that the images captured by the RPAS camera generally exhibited blooming because: (1) the microbolometer array is uncooled, (2) the 1/30th second exposure time allows for smearing associated with movement, and (3) the LWIR bandpass (8–14) is wide and includes areas of the spectrum in which hot gases in the plume may emit substantial radiation. Rectification of the imagery was made difficult by error in roll, pitch, yaw, and position (xyz) data from the aircraft. Although FRP estimates from RPAS and radiometers may have been upwardly biased, we expect that the oblique LWIR imagery from the boom-mounted FLIR camera underestimates FRP (Fig. 7). Without resorting to other information as we have done for the airborne infrared data (e.g.

full spectrum simulations of the FRFD from mixed-temperature fire pixels) (Dickinson and Kremens 2014; Kremens and Dickinson 2014), use of longwave data for estimating FRFD may always underestimate radiant emission from wildland fires because their radiant emissions peak in the midwave region of the infrared spectrum. A further potential source of downward bias for all radiation measurements reported in this paper is that, although graybody/blackbody radiation is confirmed from measurements in high transmission regions of the infrared spectrum (e.g. Johnston *et al.* 2014), measurements of spectral radiant emissions from fires suggests that radiation from hot flame gases outside high transmission regions exceeds radiation that would be predicted from graybody assumptions (e.g. Boulet *et al.* 2009, Parent *et al.* 2010). The magnitude of this bias is unknown.

Hudak *et al.* (this issue) report fuel consumption data that are likely to be the best standard against which to compare fire radiation measurements. However, consumption is proportional to fire radiative energy (Kremens *et al.* 2012), the time integral of fire radiated power (MW). Ground-based measurements of fire radiative energy from both high resolution nadir infrared cameras and radiometer data show adequate correspondence with fuel consumption (Hudak *et al.*, this issue). Fire radiated energy estimates should be more sensitive to measurement error than FRP as small biases associated with FRP measurement accumulate over the lifetime of a fire.

Our experience corroborates (Schroeder *et al.* 2013) that, if given priority, coordinating ground, airborne, and satellite measurement can result in a high rate of success. Satellite overpasses were coincident with all large block burns. Coordinating small-block firing operations with satellite overpass was successful for two fires (S5 and S6) despite satellite measurements not being a high priority in the overall measurement campaign. Though S6 FRP did not rise above MODIS background FRP, the S5 measurements coincided closely with a VIIRS image capture resulting in FRP estimates of 7.3, 7.8, and 8.0 MW for oblique LWIR, RPAS/radiometer, and VIIRS, respectively (Fig. 2). Clouds likely reduced three satellite FRP estimates. Had coincidence with satellite overpass been a top priority, we would have had added flexibility in choosing burn days that were substantially cloud free.

Conclusions

We demonstrate that obtaining FRP from coincident radiometer, oblique infrared, airborne infrared (both from piloted and remotely-piloted aircraft), and satellite sensor measurements is feasible during experimental prescribed fire operations. However, competing objectives limited opportunities for coordination of ground and airborne measurements with satellite overpass. We found that small RPAS have some utility for characterizing flame front development but their use will remain severely limited without small, lightweight, and quantitative infrared sensors and better 3D position data for image georectification. Improving confidence in the use of infrared data to estimate FRP requires a better fundamental understanding fire spectral radiation and its incorporation into measurement processes. The wide array of measurements conducted during RxCADRE 2012 provides opportunities for synthesis that have not been possible heretofore.

Acknowledgements

We thank the Eglin Air Force Base fire management staff, particularly Kevin Hiers, Brett Williams, and the fire crews for their supreme competence in prescribed burning and logistical coordination. We also thank the many scientists and support staff not included in this paper whose work and collaboration made the RxCADRE project possible, particularly Roger Ottmar who led the effort and Dan Jimenez who facilitated agreements and funding. The 2012 RxCADRE campaign was made possible by a grant from the Joint Fire Science Program (Project #11-2-1-11) while longer-term support from the US Forest Service, National Fire Plan, Joint Fire Science Program, and NASA were critical for getting the RxCADRE project started.

References

Berk A, Anderson GP, Acharya PK, Hoke M, Chetwynd J, Bernstein L, Shettle EP, Matthew MW, Alder-Golden SM (2003) MODTRAN4 version 3 revision 1 user's manual. (Massachusetts: Air Force Research Laboratory).

Boulet P, Parent G, Collin A, Acem Z, Porterie B, Clerc JP, Consalvi JL, Kaiss A (2009) Spectral emission of flames from laboratory-scale vegetation fires. *International Journal of Wildland Fire* **18**, 875–884. doi: 10.1071/WF08053

Byram GM (1959) Combustion of forest fuels. In ‘Forest fire: control and use’ (Ed KP Davis) pp. 61–89 (New York: McGraw Hill).

Coen, JL, Schroeder W (2013) Use of spatially refined satellite remote sensing fire detection data to initialize and evaluate coupled weather-wildfire growth model simulations. *Geophysical Research Letters* **40**, 5536–5541. doi: 10.1002/2013GL057868

Csiszar IA, Schroeder W, Giglio L, Ellicott E, Vadrevu KP, Justice CO, Wind B (2014) Active fires from Suomi NPP Visible Infrared Imaging Radiometer Suite: product status and first evaluation results. *Journal of Geophysical Research* **119**, 803–816. http://dx.doi.org/10.1002/2013JD020453

Dickinson MB, and Kremens RL (2014) Calibration procedure for single-band WASP LWIR data—incorporating spectral atmospheric transmission. *International Journal of Wildland Fire*, Accessory Publication available at www.xxxx.xxxx.

Ellison L, Ichoku C (2014) Alternative methods for estimating fire radiated power (MW) from MODIS observations when fire boundaries are known. *International Journal of Wildland Fire*, Accessory Publication available at www.xxxx.xxxx.

US Department of Agriculture, Forest Service Research (2014) Research data archive. http://www.fs.usda.gov/rds/archive/ [Verified xxx/xxx??]

Freeborn PH, Cochrane MA, Wooster, MJ (2014) A decade long, multi-scale map comparison of fire regime parameters derived from three publically available satellite-based fire products: a case study in the Central African Republic. *Remote Sensing* **6**, 4061–4089. doi:10.3390/rs6054061

Giglio L, Descloitres J, Justice CO, Kaufman YJ (2003) An enhanced contextual fire detection algorithm for MODIS. *Remote Sensing of Environment* **87**, 273–282. doi: 10.1016/S0034-4257(03)00184-6

Hiers JK, O'Brien JJ, Mitchell RJ, Grego JM, Loudermilk EL (2009) The wildland fuel cell concept: an approach to characterize fine-scale variation in fuels and fire in frequently burned longleaf pine forests. *International Journal of Wildland Fire* **18**, 315–325. doi:10.1071/WF08084

Hudak AT, Dickinson MB, Kremens RL, Bright BC, Loudermilk EL, O’Brien JJ, Hornsby B, Ottmar RD (In review) Measurements to relate fire radiative energy density and surface fuel consumption—RxCADRE 2011 and 2012. *International Journal of Wildland Fire* (this issue).

Johnston JM, Wooster MJ, Lynham TJ (2014) Experimental confirmation of the MWIR and LWIR grey body assumption for vegetation fire flame emissivity. *International Journal of Wildland Fire* **23**, 463–479. doi:10.1071/WF12197

Justice CO, Giglio L, Korontzi S, Owens J, Morisette J, Roy D, Descloitres J, Alleaume S, Petitcolin F, Kaufman Y (2002) The MODIS fire products. *Remote Sensing of Environment* **83**, 244–262. doi: 10.1016/S0034-4257(02)00076-7

Justice C, Giglio L, Boschetti L, Roy D, Csiszar I, Morisette J, Kaufman Y (2006) MODIS fire products—algorithm technical background document, Version 2.3. Accessed 10 May 2014 (http://modis.gsfc.nasa.gov/data/atbd/atbd_mod14.pdf).

Justice CO, Román M.O, Csiszar I, Vermote EF, Wolfe RE, Hook SJ, Fried M, Wang Z, Schaaf CB, Miura T, Tschudi M, Riggs G, Hall DK, Lyapustin AI, Devadiga S, Davidson C, Masouka EJ. (2013) Land and cryosphere products from Suomi NPP VIIRS: overview and status. *Journal of Geophysical Research, [Atmospheres]* **118**, 9753–9765. doi:10.1002/jgrd.50771

Kaufman YJ, Justice CO, Flynn LP, Kendall JD, Prins EM, Giglio L, Ward DE, Menzel WP, Setzer AW (1998) Potential global fire monitoring from EOS-MODIS. *Journal of Geophysical Research* **103**, 32215–32238. doi: 10.1029/98JD01644

Kremens RL, Dickinson MB, Bova AS (2012) Radiant flux density, energy density, and fuel consumption in mixed-oak forest surface fires. *International Journal of Wildland Fire* **21**, 722–730. doi: 10.1071/WF10143

Kremens RL, Dickinson MB (2014) Flame-front scale numerical simulation of wildland fire radiant emission spectra as a guide to wildland fire observation. *International Journal of Wildland Fire*, in review.

Kremens RL, Smith AMS, Dickinson MB (2010) Fire metrology: current and future directions in physics-based measurements. *Fire Ecology* **6**, 13–35. doi:10.4996/fireecology.0601013

Loudermilk EL, O'Brien JJ, Mitchell RJ, Cropper WP, Hiers JK, Grunwald S, Grego J, Fernandez-Diaz JC (2012) Linking complex forest fuel structure and fire behaviour at fine scales. *International Journal of Wildland Fire* **21**, 882–893. doi: /10.1071/WF10116

McKeown D, Cockburn J, Faulring J, Kremens RL, Morse D, Rhody H, Richardson M. (2004) Wildfire airborne sensor program (WASP): a new wildland fire detection and mapping system. In: Remote sensing for field users: proceedings of the Tenth Forest Service Remote Sensing Applications Conference. (Bethesda, MD: American Society of Photogrammetry and Remote Sensing). CD-ROM.

O’Brien JJ, Loudermilk EL, Hornsby B, Hiers JK, Ottmar RD (2014) High resolution infrared thermography as a tool for capturing fire behavior in wildland fires. *International Journal of Wildland Fire*, in review.

Ononye AE, Vodacek A, Saber E (2007) Automated extraction of fire line parameters from multispectral infrared images. *Remote Sensing of Environment* **108**, 179–188. doi:10.1016/j.rse.2006.09.029

Parent G, Acem Z, Lechêne, Boulet P (2010) Measurement of infrared radiation emitted by the flame of a vegetation fire. *International Journal of Thermal Sciences* **49**, 555–562. doi: 10.1016/j.ijthermalsci.2009.08.006

Peterson D, Wang J (2013) A sub-pixel-based calculation of fire radiative power from MODIS observations: 2. Sensitivity analysis and potential fire weather application, *Remote Sensing of Environment* **129**, 231–249. DOI:10.1016/j.rse.2012.10.020

Peterson D, Wang J, Ichoku C, Hyer E, Ambrosia, V (2013*b*) A sub-pixel-based calculation of fire radiative power from MODIS observations: 1 Algorithm development and initial assessment, *Remote Sensing of Environment* **129**, 262–279. DOI:10.1016/j.rse.2012.10.036

Peterson D, and Hyer E (2014) Rim Fire Overview: Fire Evolution, Meteorology, and Smoke Plumes. In review

Riggan PJ, Tissell RG, Lockwood RN, Brass JA, Pereira JAR, Miranda HS, Miranda AC, Campos T, Higgins R (2004) Remote measurement of energy and carbon flux from wildfires in Brazil. *Ecological Applications* **14,** 855–872. doi: 10.1890/02-5162

SAS Institute Inc (2013) SAS® 9.4 (Cary, NC).

Schroeder W, Ellicott E, Ichoku C, Ellison L, Dickinson MB, Ottmar R, Clements C, Hall D, Ambrosia V, Kremens RL (2013) Integrated active fire retrievals and biomass burning emissions using complementary near-coincident ground, airborne and spaceborne sensor data. *Remote Sensing of Environment* **140**, 719–730. doi: 10.1016/j.rse.2013.10.010

Schroeder W, Oliva P, Giglio L, Csiszar I (2014) The new VIIRS 375 m active fire detection data product: algorithm description and initial assessment. *Remote Sensing of Environment* **143**, 85–96. doi: 10.1016/j.rse.2013.12.008

Wolfe RE, Lin G, Nishihama M, Tewari KP, Tilton JC, Isaacman AR (2013) Suomi NPP VIIRS prelaunch and on-orbit geometric calibration and characterization. *Journal of Geophysical Research: Atmospheres* **118**, 11,508–11,521. doi: 10.1002/jgrd.50873

Wolfe RE, Nishihama M, Fleig AJ, Kuyper JA, Roy DP, Storey JC, Pratt FS (2002) Achieving sub-pixel geolocation accuracy in support of MODIS land science. *Remote Sensing of Environment* **83**, 31–49. doi: 10.1016/S0034-4257(02)00085-8

Wooster MJ, Zhukov B, and Oertel D (2003) Fire radiative energy for quantitative of biomass burning: derivation from the BIRD experimental satellite and comparison to MODIS products. *Remote Sensing of Environment* **86**, 83–107. doi: 10.1016/S0034-4257(03)00070-1

TABLES

Table 1. Fire radiative power (FRP) generated from MODIS data for the L1G, L2G and L2F burns using different methodologies

See Ellison and Ichoku (2014) for a complete characterization of the methods and their results which include consideration of pixel selection method and the method by which background FRP was determined. Here, we report the range in values obtained. The lowest value corresponds to the method in which only pixels that were significantly above background were used to generate FRP. The highest value corresponds to that obtained by combining FRP from all pixels that overlapped the burn block, thereby including radiation from pixels in which there was limited combustion. There was no saturation in MODIS data and although small burn S6 coincided temporally with MODIS overpass, the signal was lost in the background because of the large scan angle. Large burn L1G was not detected by the MYD14 methodology because of cloud effects and our manual computation of FRP is likely an underestimate. Average atmospheric transmission was used to estimate surface-leaving FRP. Whether a fire was detected (Det.) by algorithm and whether there was signal saturation (Sat.) are indicated. MODIS nadir pixel resolution is 1000 m.

Fire	Date	Time (UTC)	Scan angle (°)	Pixel area (km^2)	Top of atmosphere power		Surface leaving (corrected) power		Atm. absorp. (%)	Det.	Sat.
					Pixel	Cluster	Pixel	Cluster			
					(MW)						
S6	31 October	19:43:41	51.2	6.2	NA	NA	NA	NA	NA	N	N
L1G	04 November	19:18:58	27.9	1.5	94.4	94.9	110.4	111.0	17	N	N
L2G	10 November	18:42:01	34.0	2.0	130.1	151.4	153.8	179.3	18	Y	N
L2F	11 November	19:25:05	35.9	2.1	155.6	174.6	187.5	210.6	20	Y	N

Table 2. Specification of VIIRS fire radiative potential (FRP) retrievals for RxCADRE 2012 fires that coincided with independent FRP measurements. Atmospheric absorption of infrared radiation in the bandpass of the sensors of interest was estimated by MODTRAN and account for sensor spectral response. Because scan angles were often well off nadir, both nadir and actual pixel sizes are provided. The standard deviation associated with VIIRS power reflects variation in the multiple pixels used to characterize the background. Whether a fire was detected (Det.) by algorithm and whether there was signal saturation (Sat.) are indicated. Where signal was saturated, FRP was not estimated.

Sensor	Fire	Fire date	UTC	Nadir pixel res. (m)	Scan angle (deg)	Pixel area (km^2)	Top of atmosphere		Surface leaving (corrected)		Atm. absorp. (%)	Det.	Sat.
							Power (MW)	Std. dev.	Power (MW)	Std. dev.			
VIIRS	S5	1 November	18:15:10	375	41.5	0.275	5.95	0.09	7.96	0.11	25	Y	N
VIIRS	S5	1 November	18:15:10	750	41.5	1.1	4.23	0.70	7.66	1.23	45	N	N
VIIRS	L1G	4 November	18:59:54	375	16.4	0.16	NA	NA	NA	NA	NA	Y	Y
VIIRS	L1G	4 November	18:59:54	750	16.4	0.64	110.33	4.6	158.29	8.55	30	N	N

VIIRS	L2G	10 November	18:47:22	375	3.2	0.14	NA	NA	NA	NA	NA	Y	Y
VIIRS	L2G	10 November	18:47:22	750	3.2	0.56	108.30	4.8	150.82	8.8	28	Y	N
VIIRS	L2F	11 November	18:28:34	375	29.8	0.23	NA	NA	NA	NA	NA	Y	Y
VIIRS	L2F	11 November	18:28:34	750	29.8	0.93	153.70	6.0	236.71	10.3	35	N	N

Table 3. Fire radiative power (FRP) estimates from oblique long-wave infrared (LWIR) images of whole fires. The oblique images were obtained from a FLIR camera mounted on a 25m boom lift. Final image resolution was 1 m x 1 m after orthorectification. Total area burned includes all pixels that exceeded a background threshold of 300°K.

Fire	Active flaming duration (min)	Mean (std) number of pixels with fire (m^2)	Total area burned (ha)	FRP (MW)	
				Mean (std. dev.)	Max
S3	26	324 (286)	2.16	4.2 (3.8)	15.4
S4	20	88 (86)	0.50	1.2 (1.4)	5.5
S5	29	289 (203)	1.14	3.9 (3.0)	14.0
S7	29	150 (217)	1.14	2.1(3.3)	18.8
S8	23	353 (356)	2.31	5.1 (6.7)	41.7
S9	17	177 (173)	1.82	2.0 (2.0)	7.8

Table 4. Fire radiative power (FRP) estimates derived from remotely-piloted aircraft system (RPAS) imagery and radiometer data for fires in non-forested, small burn blocks. Frontal radiant intensities are averages from either 4 (S3, S5, S9) or 5 (S4, S7, S8) radiometers. Blocks S3–S5 were burned on 1 November 2012 while S7 and S9 were burned on 8 November 2012. It was not possible to extract perimeter data from S8 imagery.

Fire	Time (UTC)	Perimeter (m)	Frontal radiant intensity (kW m^{-1})	FRP (MW)
S3	21:29:21	1197	19.99	23.9
S4	19:38:07	204	10.87	2.2
S4	19:40:22	258	10.87	2.8
S4	19:42:44	303	10.87	3.3
S4	19:46:00	446	10.87	4.8
S4	19:50:06	454	10.87	4.9
S4	19:52:32	565	10.87	6.1
S5	18:10:28	114	26.18	3.0
S5	18:13:05	188	26.18	4.9
S5	18:13:30	212	26.18	5.6
S5	18:15:40	298	26.18	7.8
S5	18:17:59	317	26.18	8.3
S5	18:19:23	416	26.18	10.9
S5	18:20:34	402	26.18	10.5
S5	18:22:49	462	26.18	12.1
S7	17:29:02	562	54.69	30.7
S9	18:37:15	294	37.43	11.0

Table 5. Fire radiative power (FRP) estimated from airborne LWIR data from the WASP system and near-coincident MODIS (a) and VIIRS (b) data. The timing of each measurement is provided along with differences in timing and FRP between airborne and spaceborne sensors. The MODIS FRP value is the average of FRP estimated from pixel and cluster methods (see Table 2, Ellison and Ichoku 2014). An estimate of cloud cover from WASP imagery is available for L1G satellite overpasses. The piloted aircraft was lower than the cloud deck during L2F so no estimate of cloud cover was made.

a. VIIRS

Fire	FRP (MW)			Cloud	Time (UTC)		
	WASP	MODIS	Diff		WASP	MODIS	Diff (s)
L1G	148	111	37	Yes (5%)	19:19:47	19:18:58	49
L2G	111	167	-55	No	18:42:26	18:42:01	25
L2F	119	199	-80	No	19:25:56	19:25:05	51
		Mean (SD)	-33 (62)				

b. VIIRS

Fire	FRP (MW)			Cloud	Time (UTC)		
	WASP	VIIRS	Diff		WASP	VIIRS	Diff (s)
L1G	414	158	256	Yes (2%)	18:59:24	18:59:54	30
L2G	152	151	1	No	18:49:08	18:47:22	106
L2F	487	237	250	Yes	18:29:47	18:28:34	73
		Mean (SD)	169 (146)				

Fig. 1. Small and large burn blocks for which data are presented in this paper. For large burn blocks, fire radiative power (FRP) (MW) was estimated from LWIR data from the WASP sensor flown on a piloted aircraft and from satellite sensors (MODIS and VIIRS). For small burn blocks, FRP was estimated from a combination of data from dual-band radiometers and a LWIR camera flown on a remotely-piloted aircraft system (RPAS). RPAS-based FRP estimates were compared with estimates derived from data from a LWIR camera with an oblique perspective of the fires. Fire in one small burn block (S5) also coincided with a VIIRS overpass. Block L2F was forested while the vegetation on the other blocks was a mix of herbs and shrubs.

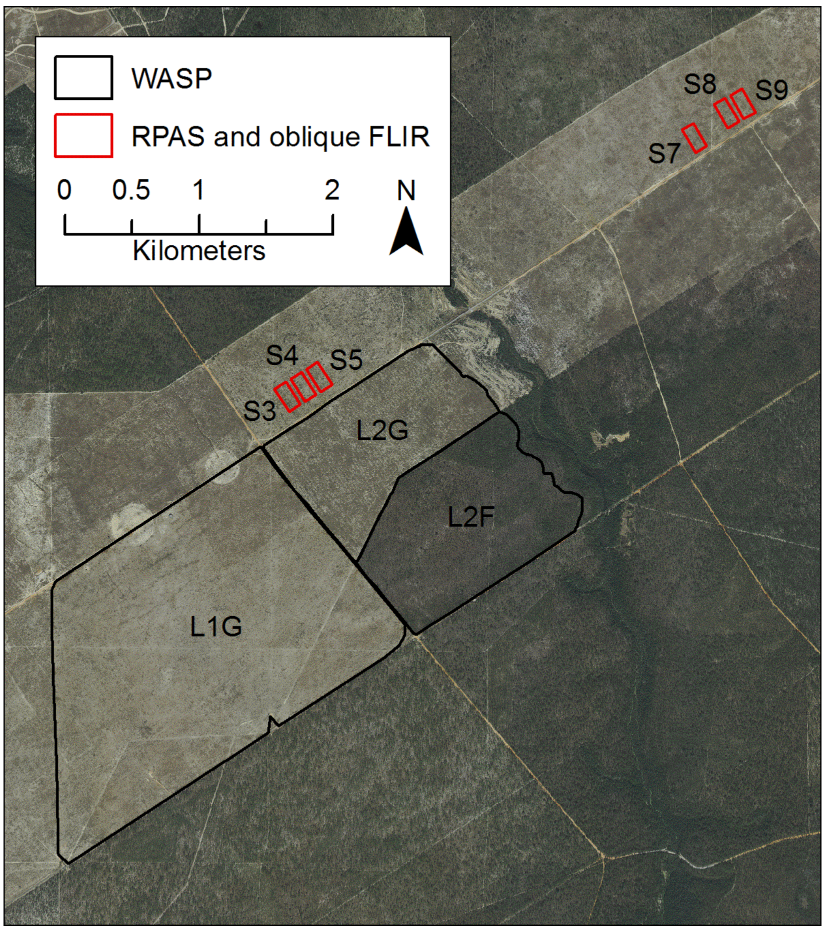

Fig. 2. RPAS LWIR image from the FLIR Tau 640x480 camera at 18:15:40 UTC for fire in burn block S5 overlain with successive perimeters and underlain by a high-resolution orthophoto. Surveyed hot targets are visible in the infrared image with white being relatively hot and black being cool. Note evidence of prior burnout along the eastern perimeter. The G2R captured images used to extract perimeters from a southerly perspective at 600 ft AGL. Shown are successive perimeters drawn from infrared images at 18:10:28 (teal), 18:13:05 (purple), 18:13:30 (green), 18:15:40 (red), 18:17:59 (orange), and 18:22:49 (yellow).

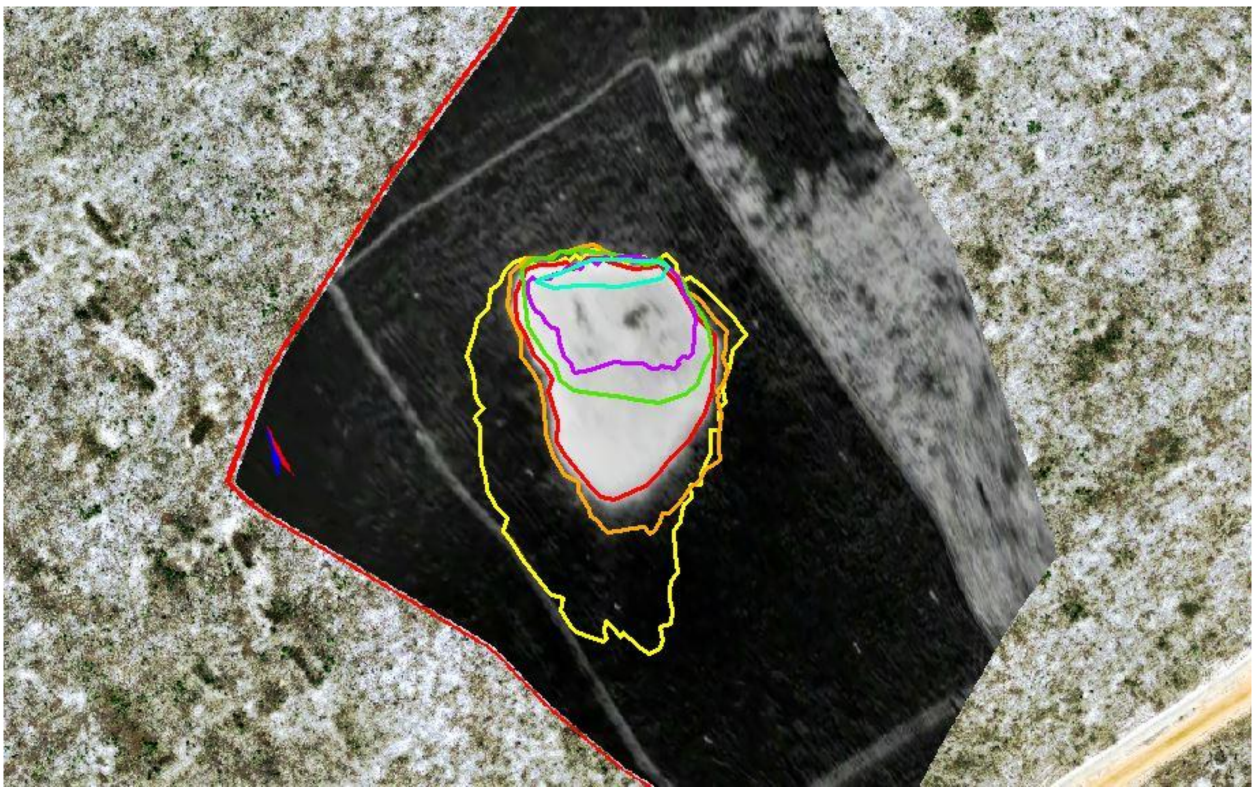

Fig. 3. Whole-fire FRP derived from oblique LWIR data for block S5. The second peak coincides with burnout around the downwind perimeter after the main heading fire had approached the unit boundary. Also shown is coincidence among RPAS-, oblique infrared-, and VIIRS-based estimates of FRP. The oblique infrared and VIIRS estimates are coincident temporally while the RPAS estimate is 30 s after the VIIRS estimate.

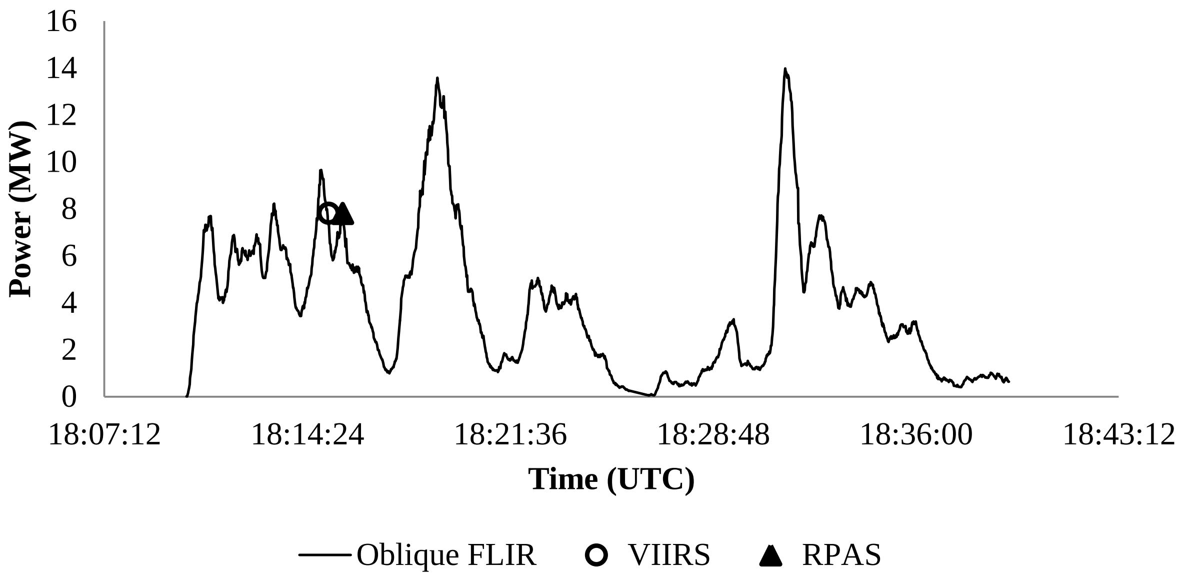

Fig. 4. Time-course of whole-fire FRP derived from WASP LWIR imagery and associated satellite measurements. Temporal autocorrelation (Table 5) was estimated from these data and from oblique FLIR data shown in Fig. 2. Shown is the mean and upper and lower 95% confidence limits in FRP arising from variation in estimates of background FRFD. Satellite measurements are within 2 min of the closest WASP measurements (Table 5). FRP for L1G for both MODIS and VIIRS and L2F for VIIRS is expected to be underestimated due to partial cloud obscuration. Pixel and cluster methods for MODIS FRP estimation are described in Ellison and Ichoku (2014).

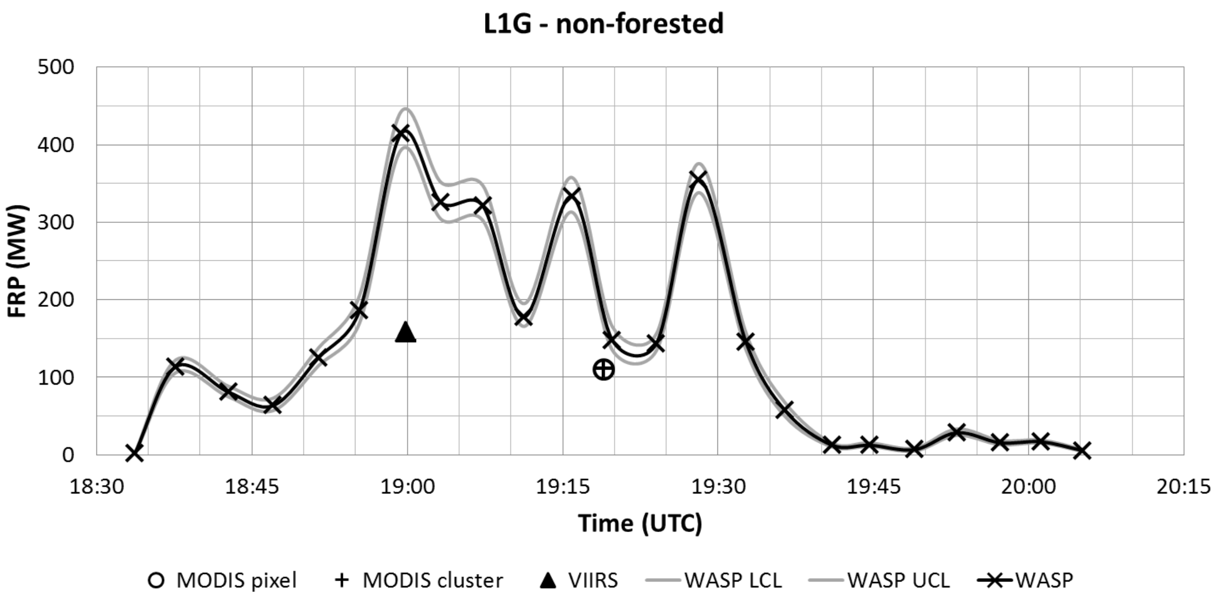

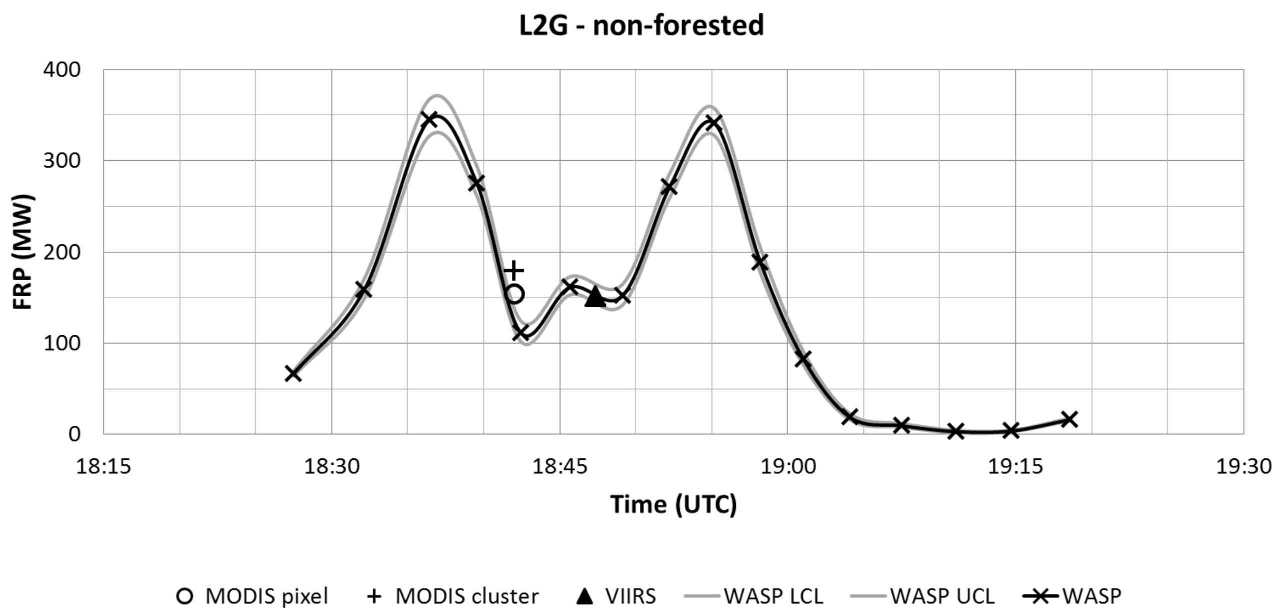
L2G - non-forested
400
300
200
100
0
FRP (MW)
18:15
18:30
18:45
19:00
19:15
19:30
Time (UTC)
MODIS pixel
MODIS cluster
VIIRS
WASP LCL
WASP UCL
WASP

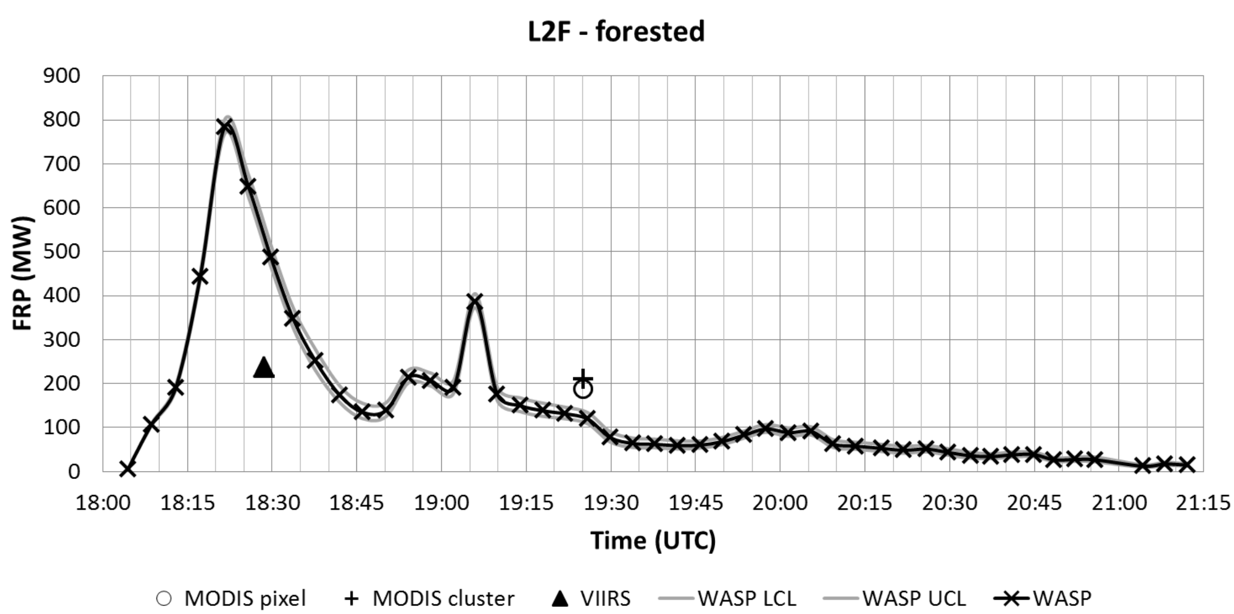
L2F - forested
900
800
700
600
500
400
300
200
100
0
FRP (MW)
18:00
18:15
18:30
18:45
19:00
19:15
19:30
19:45
20:00
20:15
20:30
20:45
21:00
21:15
Time (UTC)
MODIS pixel
MODIS cluster
VIIRS
WASP LCL
WASP UCL
WASP

Fig. 5. Near-coincident WASP LWIR mosaic (background green-red) overlain by MODIS (nominal 1000 m) and VIIRS (nominal 375 m) active fire masks for burn block L2F. Satellite pixels are displayed according to fire algorithm output classification (thick/dashed = fire detections; magenta = clouds; thin/solid = clear land pixel). Note that the WASP mosaic may miss some heat from near the upper block boundary. All figures show the WASP infrared mosaic that was closest in timing (shown) to the satellite overpass.

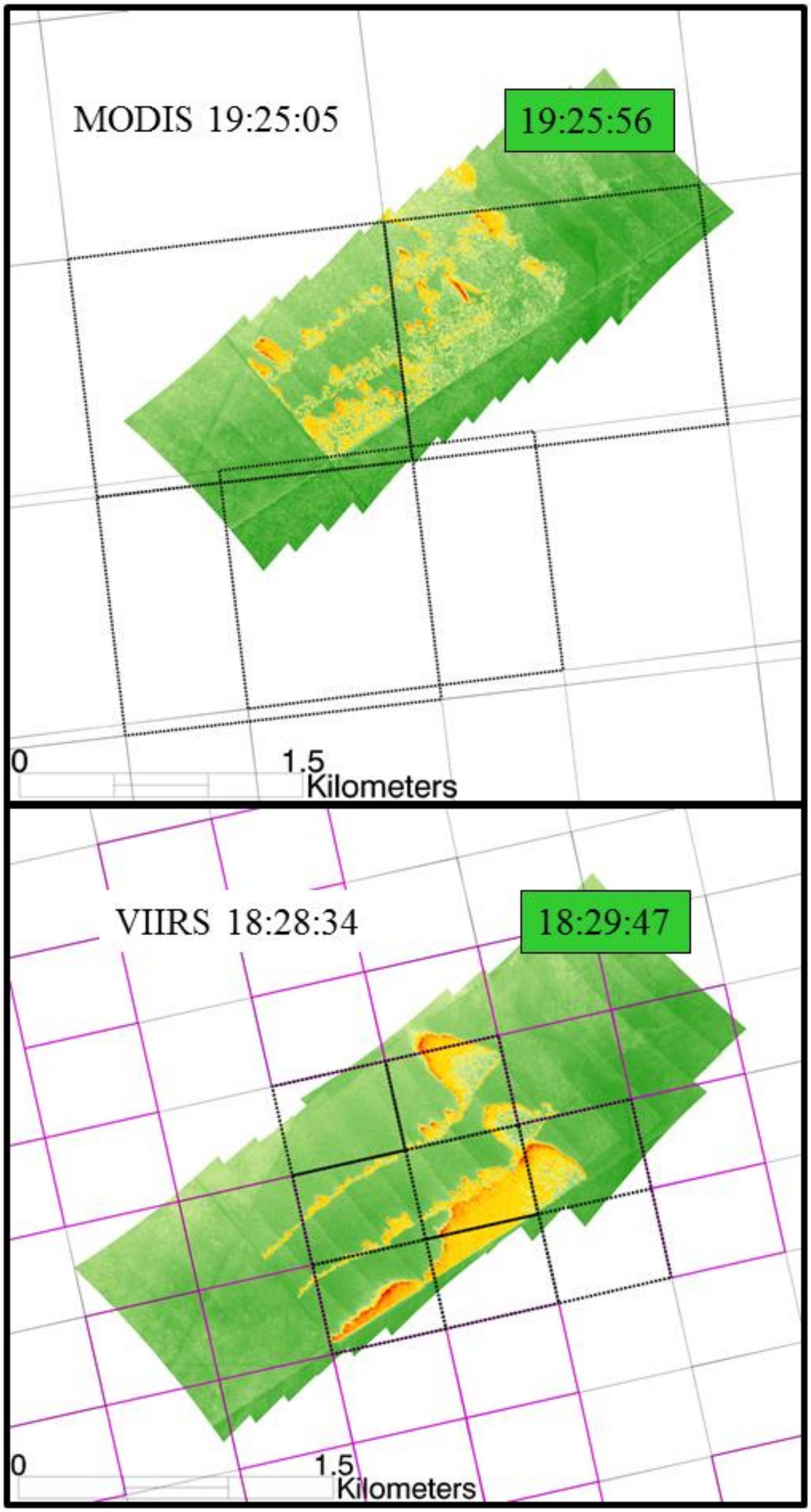

MODIS 19:25:05
19:25:56
0
1.5
Kilometers
VIIRS 18:28:34
18:29:47
0
1.5
Kilometers

Fig. 6. Comparisons of MODIS and VIIRS estimates of FRP with the estimate from WASP LWIR data that is closest to it in timing. The 1:1 reference line is provided. The range in MODIS measurements from the pixel and cluster methods is shown along the x-axis (see Table 1, Ellison and Ichoku 2014). The range for L1G is small because cloud cover prevented all pixels that overlapped the burn block from being included in the cluster FRP estimate. Both MODIS and VIIRS measurements are corrected for atmospheric absorption. The 95% confidence interval in WASP measurements resulting from variation in estimates of background FRFD is shown on the y-axis. MODIS and VIIRS measurements for L1G were affected by clouds along with the VIIRS measurement for L2F.

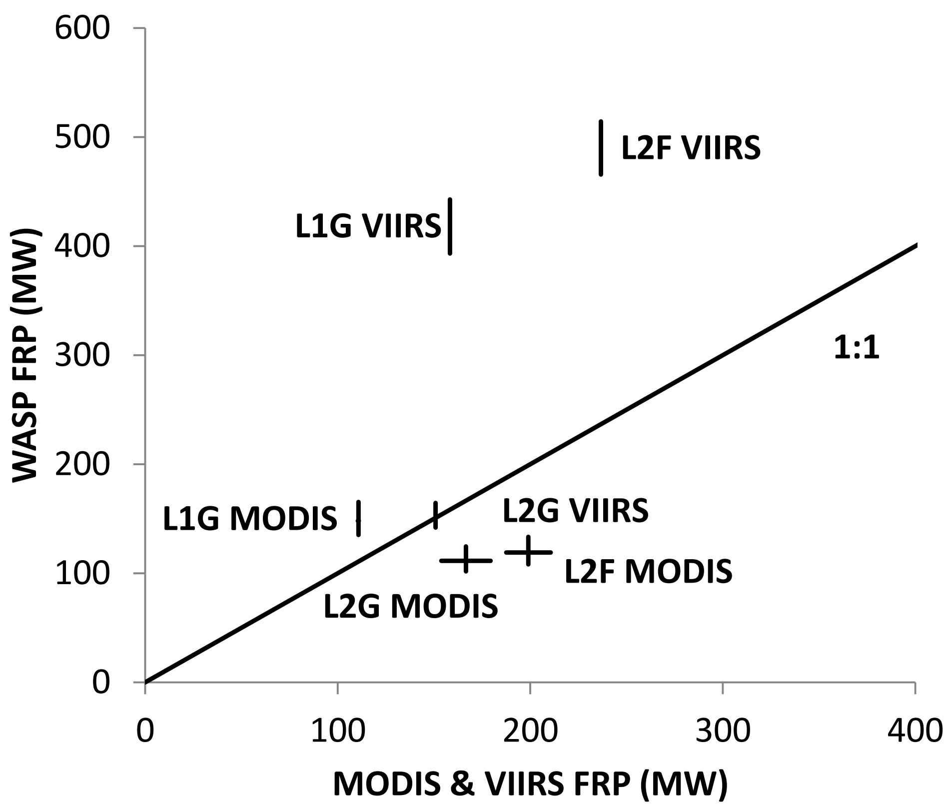

Fig. 7. Comparison of oblique longwave infrared and RPAS-based estimates of FRP. Oblique FLIR data were collected from a boom lift outside the fire perimeter. To obtain FRP, fire perimeters (m) derived from RPAS imagery were multiplied block-average fire radiant intensity (kW m^{-1}) estimated from dual-band radiometer data. The 1:1 expectation reference line is provided.